ACS SENSORS

pubs.acs.org/acssensors

Article

Electrochemical Impedance Spectroscopy Biosensor Enabling Kinetic Monitoring of Fucosyltransferase Activity

Viktoria Heine, Tom Kremers, Nora Menzel, Uwe Schnakenberg,* and Lothar Elling*

Cite This: *ACS Sens.* 2021, 6, 1003−1011

Read Online

ACCESS | Metrics & More | Article Recommendations | Supporting Information

ABSTRACT: Monitoring glycosyltransferases on biosensors is of great interest for pathogen and cancer diagnostics. As a proof of concept, we here demonstrate the layer-by-layer immobilization of a multivalent neoglycoprotein (NGP) as a substrate for a bacterial fucosyltransferase (FucT) and the subsequent binding of the fucose-specific *Aleuria aurantia* lectin (AAL) on an electrochemical impedance spectroscopy (EIS) sensor. We report for the first time the binding kinetics of a glycosyltransferase in real-time. Highly stable EIS measurements are obtained by the modification of counter and reference electrodes with polypyrrole: polystyrene sulfonate (PPy:PSS). In detail, the *N*-acetyllactosamine (LacNAc)-carrying NGP was covalently immobilized on the gold working electrode and served as a substrate for the FucT-catalyzed reaction. The LacNAc epitopes were converted to Lewis^x (Le^x) and detected by AAL. AAL binding to the Le^x epitope was further confirmed in a lectin displacement and a competitive lectin binding inhibition experiment. We monitored the individual kinetic processes via EIS. The time constant for covalent immobilization of the NGP was 653 s. The FucT kinetics was the slowest process with a time constant of 1121 s. In contrast, a short time constant of 11.8 s was determined for the interaction of AAL with the modified NGPs. When this process was competed by 400 mM fucose, the binding was significantly slowed down, as indicated by a time constant of 978 s. The kinetics for the displacement of bound AAL by free fucose was observed with a time constant of 424 s. We conclude that this novel EIS biosensor and the applied workflow has the potential to detect FucT and other GT activities in general and further monitor protein−glycan interactions, which may be useful for the detection of pathogenic bacteria and cancer cells in future biomedical applications.

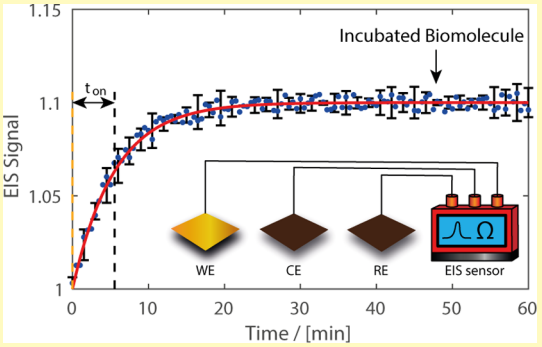

KEYWORDS: *biosensor, electrical impedance spectroscopy, neoglycoprotein, fucosyltransferase, lectin*

Biosensors play a crucial role in various biological and biomedical applications because they enable the detection of proteins, toxins, or microorganisms. Host−pathogen interaction and cancerogenesis often comprise the glycan−lectin interplay. This process is taken advantage of in many biosensor applications to facilitate, for example, drug development and diagnostics. Aside from methods such as frontal affinity chromatography, microarrays, or enzyme-linked lectin assays, electrochemical impedance spectroscopy (EIS) is a highly sensitive and commonly used method to investigate such glycan−lectin interactions.[1] Several glycan-based EIS sensors were elaborated in the past. Cui et al.[2] developed a mannose-coated gold sensor to capture the bacteria *S. typhimurium* ATCC14028, *Escherichia coli* JM109, and *E. coli* DH5*α*. Sialylated oligosaccharide-coated biosensors selectively detected the *Maackia amurensis* agglutinin[3] and were able to distinguish between different types of the avian influenza virus.[4] In our previous work, we determined the thickness of glycopolymer brushes via EIS[5] and combined it with surface plasmon resonance to further investigate the lectin−glycan interactions[6] and the binding of the *Clostridium difficile* toxin TcdA receptor domain to the Galili epitope.[7] In all these applications, a multivalent glycan presentation was created directly on the gold sensor surface. To take glycan multivalency to the near-natural level, integration of a second scaffold is necessary. Bovine serum albumin (BSA)-based neoglycoproteins (NGPs) were used in various applications as a scaffold for the multivalent glycan presentation.[8,9] In our study, NGPs are especially interesting because pathogenic or cancerogenic carbohydrate-binding proteins (lectins) exhibit strong binding to multivalently presented glycan structures because of their oligomeric carbohydrate recognition domain.[8,9] We already showed that the post-modification of immobilized NGPs via glycosyltransferases (GTs) is a feasible method to screen for novel glycan ligands of bacterial toxins.[8] Disease-related glycan epitopes (e.g., Lewis group antigens)

Received: October 22, 2020
Accepted: January 25, 2021
Published: February 17, 2021

https://dx.doi.org/10.1021/acssensors.0c02206
ACS Sens. 2021, 6, 1003−1011

Scheme 1. Schematic Workflow of the Performed Experiments in This Study[a]

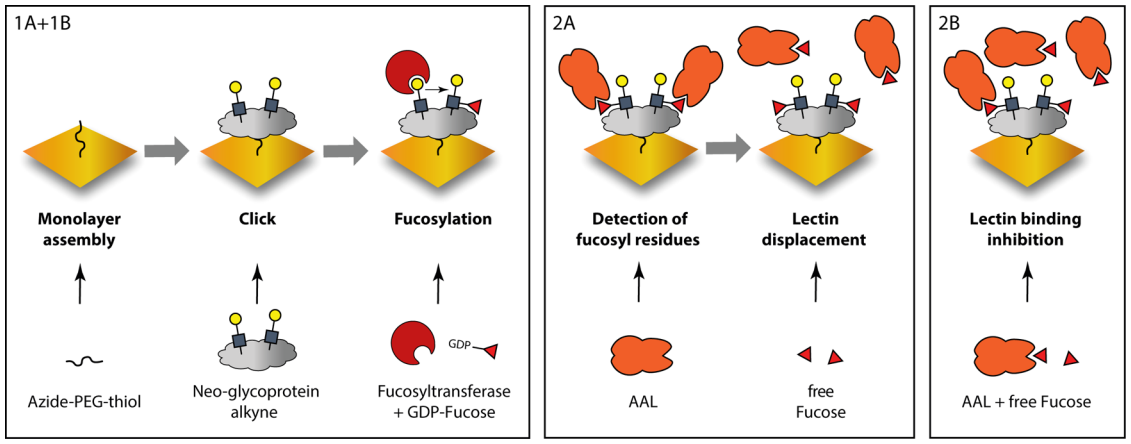

[a]Experiment 1A: A SAM was bound to the WE gold surface, and LacNAc-NGPs were immobilized on the EIS sensor via click chemistry. Experiment 1B: Incubation of FucT on the NGPs with the donor substrate GDP-fucose. Experiment 2A: The attached fucose was detected via the fucose-specific lectin AAL. The bound lectin was displaced via addition of free fucose as further verification of the fucosylation reaction. Experiment 2B: AAL and free fucose were applied simultaneously to the primed sensor chips in a lectin-binding inhibition experiment where free and bound fucose compete for AAL binding.

were synthesized by a set of GTs present in pathogenic bacteria (e.g., *Helicobacter pylori*)[10] or overexpressed in cancer cells.[11,12] Monitoring GT activities on a biosensor is therefore highly in demand to detect infections or cancer. On-sensor chip modification of multivalent NGPs by a galactosyltransferase and subsequent lectin binding was reported using a sandwich-electrogenerated chemiluminescence biosensor.[13] Enzyme activity was detected by binding of the galactose-specific *Erythrina cristagalli* lectin using cyclic voltammetry (CV) and EIS.

EIS is widely used to obtain real-time information about binding processes, for example, for detection of molecular binding processes such as the protein−protein or lectin−glycan interaction, virus detection, and DNA sensing.[5−7,14−21] In contrast to fluorescence techniques, EIS is label-free. To ensure a high sensitivity in the vicinity of the surface, commonly interdigitated electrodes (IDEs) are utilized confining the electric field close to the sensor surface.[22] Recently, a combination of IDEs, where one finger, the working electrode (WE), is made from gold and the adjacent finger, the combined counter electrode (CE) and pseudo-reference electrode (RE), is coated with the conducting polymer polypyrrole (PPy) doped with polystyrene sulfonate (PSS) (PPy:PSS), were applied to monitor binding of proteins to a thiolated self-assembling monolayer (SAM) immobilized on the gold finger electrode.[23,24] On the one hand, PPy:PSS coating increases the reproducibility of the measurements in a two-electrode arrangement; on the other hand, thiol-based molecules do not bind to PPy:PSS surfaces.[23,24]

In this study, we present for the first time the subsequent kinetic binding analysis of a bacterial fucosyltransferase (FucT) and the fucose (Fuc)-specific lectin AAL to the synthesized Lewis^x (Le^x) antigen epitope. Scheme 1 shows the general buildup of the layers on the gold sensors. The WE gold surface was first modified by a SAM carrying azide groups. An alkyne-modified NGP carrying *N*-acetyllactosamine (LacNAc) glycans was then conjugated via a copper-catalyzed alkyne azide cycloaddition (CuAAC) (experiment 1A). Subsequently, fucosylation of NGP was performed by incubation with the bacterial FucT and GDP-fucose (experiment 1B). NGP immobilization and fucosyltransfer were monitored by sugar-specific lectins and EIS sensing (experiment 2A and 2B). This work presents for the first time the kinetic binding analysis of a GT. The new biosensor approach has the potential as a diagnostic tool for the detection of FucT-expressing pathogenic bacteria and to set up an NGP library on-chip to monitor binding kinetics of GTs during elongation of the sugar chains.

MATERIALS AND METHODS

Preparation of Enzymes. The GTs β4-galactosyltransferase from humans (β4GalT) and the α3FucT from *H. pylori* (α3FucTΔ52 with quadruple point mutations) were prepared as described before.[8,25,26] Briefly, *E. coli* BL21 (DE3) pLysS was transformed with the respective plasmids (synthesized by GeneArt, Thermo Fisher Scientific, Waltham, MA, USA, and BioCat, Heidelberg, Germany), and cells were cultivated in a terrific broth medium and induced with 0.5 mM IPTG at an OD_{600} of 0.6−0.8. Purification of the enzymes was performed with immobilized metal ion affinity chromatography (IMAC) (HisTrap columns, GE Healthcare, Chicago, IL, USA) using the buffers recommended by the manufacturer. After elution, the FucT fraction was dialyzed with 50 mM Tris buffer (pH 7.4) containing 500 mM NaCl.

Production of Neoglycoproteins. In the first step, Galβ1,4Glc-NAc-(LacNAc)tBoc was produced from its precursor GlcNAc-tBoc. The latter was synthesized chemically as described by Sauerzapfe et al.[27] and treated with the β4GalT.[25,28] Analysis of the reaction and purification of the reaction product were performed with reversed-phase HPLC (Dionex system; ThermoFisher Scientific, Darmstadt, Germany). An analytic MultoKrom 100−5 C18 column (250 mm × 4 mm; CS Chromatographie, Langerwehe, Germany) was applied with a flow rate of 1 mL/min (isocratic eluent of 15% acetonitrile and 85% water). The product LacNAc-tBoc was deprotected and coupled to squaric acid diethyl ester as described in a previous publication.[28] Squarate monoamide esters (LacNAc−squarate), carrying the glycan, were separated from free squaric acid diethyl ester via RP-HPLC (see above, flow 0.5 mL/min). The LacNAc−squarate product synthesis was confirmed by electron spray ionization−mass spectrometry (ESI−MS) (Figure S1) on a Multospher 120 RP 18 HP-3μ column (60 mm × 2 mm; CS Chromatographie, Langerwehe, Germany) with a Finnigan Surveyor MSQ Plus (ThermoFisher Scientific, Darmstadt, Germany) and a flow rate of 0.2 mL/min with 50% acetonitrile as a mobile phase (needle voltage = 4 kV, temperature = 400 °C, cone voltage = 100 V, negative mode). For the coupling of the squarate

https://dx.doi.org/10.1021/acssensors.0c02206
ACS Sens. 2021, 6, 1003−1011

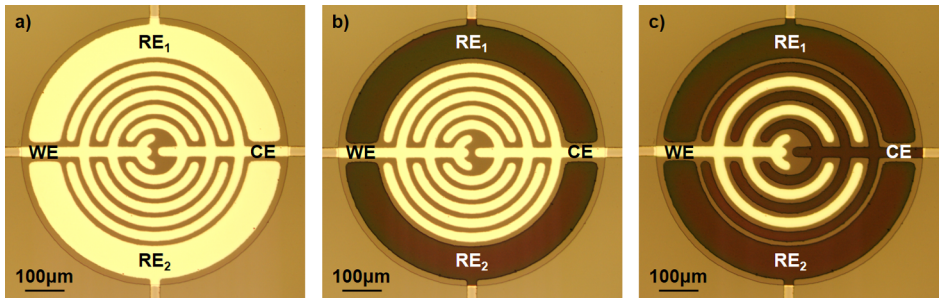

Figure 1. (a) Microscopy pictures of interdigitated gold electrodes with lines and spaces of 20 μm each surrounded by two large gold electrodes. A thin layer of Parylene C and Teflon protects the whole chip and is circularly opened in the sensor area. (b) In a first step, RE_1 and RE_2 are coated with PPy:PSS (Q = 300 μC) by a potentiostatic electropolymerization process. PPy:PSS electrodes exhibit a brownish color. (c) CE modified by electrodeposition of PPy:PSS (Q = 170 μC). The contact leads remain uncoated because of their electrical insulation by Parylene C and Teflon.

monoamide esters to BSA or the alkyne-functionalized BSA (see below), occupation of 20 lysine residues per molecule BSA was pursued.[28] BSA (60 μM) was mixed with 1.2 mM LacNAc−squarate in 50 mM sodium tetraborate buffer pH 9.2 and incubated by shaking for 72 h. The occupation of the BSA molecules with glycan residues was estimated by an SDS-PAGE (8%) via the altered molecular weight (Figure S2, Table S1).

Immobilization of Neoglycoproteins on Gold Chips. All solutions for the layer assembly were supplemented by 0.05% (w/v) Pluronic F68 (BASF, Ludwigshafen, Germany) (designated, e.g., as PBSp) to remove unspecifically bound compounds during rinsing and to prevent biofouling on the sensor chips.[29] The immobilization of proteins to the gold surface was performed using click chemistry via CuAAC. The BSA and NGPs were functionalized with an NHS-PEG-alkyne linker (tebu-bio GmbH, Le Perray-en-Yvelines, France) as previously described.[30] First, the linker was incubated (in excess, 1.1-fold) with 30 μM BSA or NGP in phosphate-buffered saline (PBS, pH 7.4) for 1.5 h at room temperature. The modified proteins were separated from the remaining reagents by ultrafiltration. For protein immobilization on gold surfaces, oxidized silicon wafers were coated with a 30 nm titanium (Ti) layer and a 100 nm gold (Au) layer by sputter deposition and diced into 3.5 mm × 3.5 mm chips serving as the scaffold. The gold surface of the chips was coated with azide-PEG-thiol (Interchim, Montluçon, France) [0.5 mM in 50% (v/v) ethanol] for 30 min. Alkyne-functionalized BSA was further biotinylated as described by the manufacturer (EZ-Link Sulfo-LC-LC-NHS-Biotin, Thermo Fisher Scientific, Waltham, MA, USA) and served as a control for the CuAAC reaction. After washing with PBST (PBS containing 0.02% Tween), alkyne-functionalized BSA or NGP (10 μM, 50 μL) in PBS (pH 7.4) supplemented with 5 mM sodium ascorbate, 0.5 mM THPTA, and 0.1 mM $CuSO_4$ for the CuAAC reaction was applied to the chips and incubated for another 30 min.[30,31]

Sensor Fabrication. EIS biosensors were fabricated on 4″ borosilicate glass wafers (Siegert Wafer GmbH, Aachen, Germany). Negative photoresist AZ nLOF 2070 (MicroChemicals GmbH, Ulm, Germany) was spin-coated and patterned by standard UV-photolithography. Subsequently, an adhesion layer (30 nm Ti), the electrode material (220 nm Au), and a 50 nm Ti protective layer were sputtered in a Nordiko NS 2550 sputtering system followed by a lift-off process. For insulation, a thin layer of Parylene C (PDS 2010 E LabCoter 1, Specialty Coating Systems, Indianapolis, IN, USA) was deposited. Teflon AF 1600 (The Chemours Company, Wilmington, DE, USA) was spin-coated on top and cured. The sensor spot (diameter 750 μm) was opened by a second photolithography step followed by reactive ion etching in an oxygen atmosphere. Finally, the Ti protective layer on top of the gold was removed by wet etching in an ammonium hydroxide−hydrogen peroxide solution just before the experiments to obtain clean sensor surfaces. Figure 1a shows the gold electrodes after the cleanroom fabrication processes. High sensing stability is facilitated by the use of an on-chip pseudo-RE made of PPy:PSS in a three-electrode setup in combination with a gold WE and a PPy:PSS CE. Therefore, the CE as well as RE were subsequently coated with the conducting polymer PPy:PSS employing electropolymerization as described by El Hasni et al. and Kremers et al.[24,32] Briefly, a 200 μL droplet containing 100 mM pyrrole and 100 mM PSS was pipetted onto the electrode area. First, the two RE areas (RE_1 and RE_2) were coated by applying a potential of 1 V to both RE areas, while the CE and WE were connected to the ground. A charge Q of 300 μC was transferred during deposition scaling with the amount of polymer.[33−35] The sensor area after the first deposition is depicted in Figure 1b. Second, the CE was coated by applying the potential versus the grounded WE (Q = 170 μC). After both depositions, the chip was cleaned by rinsing with deionized water and isopropanol and finally dried under a stream of nitrogen. Figure 1c shows the final sensor design including labels for the specific electrodes.

EIS Measurements. Transient EIS measurements were carried out using the three-electrode arrangement in combination with a Hewlett Packard 4294A Precision Impedance Analyzer (Palo Alto, CA, USA). For the measurements, the two parts of RE were shorted as described above. A 5 μL droplet of each solution was dispensed on a hydrophobic Teflon-coated bottom plate. The top plate with the EIS sensor was fixed in 130 μm distance to the bottom plate separated by Parafilm-M as a spacer. Electrical impedance values at a voltage amplitude of 10 mV were recorded. Impedance spectra were taken approximately every minute for 1 h per incubation step. The imaginary part of the impedance was evaluated at a frequency of 400 Hz to monitor binding events on and in the vicinity of the electrode surface. At the chosen frequency, the double-layer capacitance dominates the electrochemical impedance leading to nonfaradaic EIS.[36] After every incubation, the sensor chip was rinsed with PBSp and dried gently under a stream of nitrogen to remove unspecifically bound molecules. Table 1 lists the single incubation steps on the chips, comprising reaction conditions and experiment code, as already introduced in Scheme 1. Displacement (2A) and competitive inhibition (2B) of AAL were performed in two separate experiments.

Table 1. Subsequent Steps of Layer Build-Up on Gold Chips, Including Used Buffers and Concentration of Compounds[a]

experiment	step	buffer	concentration
1A	NGP	PBSp, 5 mM sodium ascorbate, 0.5 mM THPTA, 0.1 mM $CuSO_4$	10 μM
1B	FucT	50 mM Tris/HCl pH 7, 25 mM KCl, 25 mM $MgCl_2$, 1 mM GDP-Fuc, 20 μL/mL FastAP, 150 μg/mL FucT	150 μg/mL
2A	AAL	PBSp	0.5 μg/mL
	Fuc	water	400 mM
2B	AAL + Fuc	1:1 PBSp/water	0.5 μg/mL, +400 mM

[a]Solutions were applied in 5 μL entities.

https://dx.doi.org/10.1021/acssensors.0c02206
ACS Sens. 2021, 6, 1003−1011

Electrode Cleaning. Before each experiment, the electrodes were cleaned in a solution of deionized water, ammonium hydroxide (NH_4OH, 25%, Th. Geyer GmbH & Co. KG, Renningen, Germany), and hydrogen peroxide (H_2O_2, 30%, MicroChemicals GmbH, Ulm, Germany) in the volume ratio of 7:2:1 for 60 min. The ability of this cleaning step to obtain a clean surface was recently confirmed by EIS and CV.[24,37] Also, the treatment is able to remove the residual thiol-bound biomolecules from the gold surface.[38] It is noteworthy that the PPy:PSS coatings were removed as well during the cleaning step and need to be prepared before each assay. This is advantageous because standardized initial conditions of the sensor are crucial in making the measurements comparable.

Rate Constant Computation. For kinetic information, the evolution of the imaginary part of the electrical impedance obtained at a frequency of 400 Hz is first normalized to the initial value. Subsequently, the normalized curves were fitted to an exponential function of the first order according to

$$\frac{\mathrm{Im}(Z)}{\mathrm{Im}(Z_0)} = A\cdot(1 - \mathrm{e}^{-k_{on}\cdot t}) + 1 \quad (1)$$

where A is the relative change of the signal and k_{on} is the rate constant. It is important to denote that the unit of k_{on} given in the functions provided in the inset of the graphs is "per second" (s^{-1}), unless it is indicated otherwise in the text. In addition, we define the time constant of the reaction as the inverse rate constant according to

$$t_{on} = \frac{1}{k_{on}} \quad (2)$$

The time constant can be interpreted as the duration where $1 \times e^{-1}$ (63.2%) of the signal change occurs. Saturation of the exponential function can be assumed when $3 \times t_{on}$ elapsed (95%).

RESULTS

In this study, we established a robust protocol for the conjugation of NGPs to monitor the kinetic binding of a bacterial FucT on an EIS sensor (Scheme 1). We took advantage of the CuAAC-mediated covalent coupling of NGPs directly to the gold surface. Azide-PEG-thiol was incubated on the gold chips; the thiol interacts with the gold surface and builds a SAM with the exposed azide groups. The alkyne part of this reaction was attached to the NGP. The protocols for the modifications of the gold chips were optimized in microtiter plates as described in the Supporting Information.

To gain information about the kinetics of each step, EIS measurements were carried out as described above. The azide SAM was first bound to the bare gold surface of the WE, followed by incubation in the buffer that was used during the following steps for 60 min. During this incubation, EIS measurements were conducted to obtain a stable electrode behavior by settling of the OCP: the exposure of the electrodes to a salt-containing solution results in ion trapping in the pores of the PPy:PSS layers causing a change in the electrochemical equilibrium.[24] For subsequent measurements, it is advantageous to wait until a steady state is reached. Thus, signal drift, especially on RE, can be prevented for subsequent measurements.

A set of different experiments was monitored by EIS on azide SAM-pretreated sensors. In the experiments 1A and 1B (Scheme 1 and Table 1), the immobilization of NGP on SAMs and subsequent incubation with FucT (5 times each) to generate Le^x-NGP was investigated. In the following experiment 2A (Scheme 1 and Table 1), the binding of AAL to the Le^x-NGP was monitored, followed by the displacement of bound AAL (0.5 μg/mL) by incubation of 400 mM Fuc (5 times). In experiment 2B (Scheme 1 and Table 1), the presence of Fuc competed the binding of AAL (0.5 μg/mL) to the Le^x-NGP (5 times).

Figure 2 shows the evolution of the imaginary part of the electrical impedance during incubation of NGP (experiment

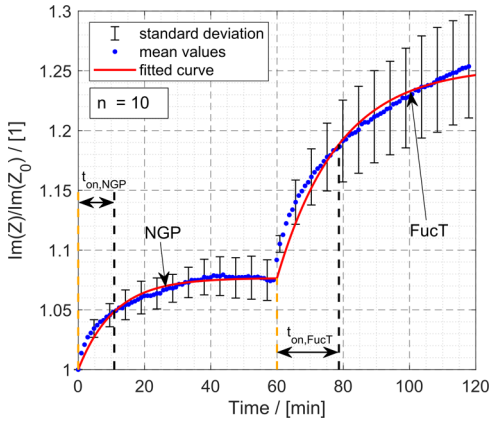

Figure 2. Temporal development of the imaginary part of the electrical impedance during NGP and subsequent FucT incubation (experiment 1A and 1B). The imaginary signal part at 400 Hz is normalized to the first value of each incubation step. For the FucT incubation (starting at 60 min), the obtained value is multiplied with the last value after NGP incubation. The values are averaged and the standard deviation is indicated by error bars (n = 10). t_{on} values for each incubation step are depicted in the graphs. The fitted exponential functions of both incubation steps are depicted in the Supporting Information (Figures S6 and Figure S7).

1A) and FucT (experiment 1B) for 60 min each at a frequency of 400 Hz. All 10 measurements for each experiment were averaged, and the standard deviations were added in the form of error bars. A Bode plot of an impedance spectrum recorded at the beginning of NGP incubation is presented in the Supporting Information (Figure S4). The evaluated frequency of 400 Hz is highlighted, showing that the electrical impedance is dominated by the double-layer capacity in this frequency regime (phase angle approaches −90°). The imaginary part of the impedance is here inversely proportional to the electrical double-layer capacity.[39] Thus, the imaginary signal part at 400 Hz is a suitable measure for monitoring immobilization processes on the gold WE. In addition, Nyquist diagrams before and after NGP incubation are exemplarily shown in Figure S5. The semicircle correlating with charge transfer is suppressed because of the lack of redox couples in the buffer solutions. Due to immobilization of the NGP on the WE, the impedance of the double layer increases because of a prolonged distance of the counter charges from the electrode in the electrical double layer.

Upon application of the NGP, the signal increases and saturates at a value of around 1.077. After rinsing and drying, as described above, the FucT incubation is monitored with an increasing impedance signal, indicating fucosylation of the NGP. It is noteworthy that every incubation period was normalized to the first value of the corresponding incubation step. For a total overview of the entire stack buildup, the initial value of each incubation step (always equal unity) was multiplied with the final value of the signal before. For FucT, compared to the NGP, the signal increase is higher in magnitude but does not saturate after 60 min. However, for both parts, rate constants according to eq 1 have been derived. Plots for both single incubation steps including the fitted

https://dx.doi.org/10.1021/acssensors.0c02206
ACS Sens. 2021, 6, 1003−1011

exponential function are depicted in the Supporting Information (Figures S6 and S7). According to eq 2, the time constant for NGP was calculated to be $t_{on,NGP}$ = 653 s and for FucT $t_{on,FucT}$ = 1121 s (Table 2), respectively.

Table 2. t_{on} and t_{off} Values for the Single Steps in EIS Measurements

experiment	step	t_{on} [s]	t_{off} [s]
1A	NGP coupling	653	
1B	FucT incubation	1121	
2A	AAL binding	11.8	
	displacement of bound AAL by Fuc incubation		424
2B	competitive binding of AAL in the presence of Fuc	978	

After FucT incubation, five samples were first exposed to AAL and then incubated with Fuc for 1 h each (experiment 2A). During incubation of AAL, a flat line occurred on average (Figure S8). As already mentioned, the impedance spectra were taken approximately every minute, which might cause undersampling for the AAL incubation step. To further resolve the first 5 min of AAL incubation, in addition to the experiments described before, electrodes were cleaned, PPy:PSS was deposited, and azide-SAM, PBSp, NGP, and FucT were incubated. The AAL was then incubated on the WE, and the sampling rate of the EIS measurement was significantly increased by a factor of about 50. Figure 3 shows

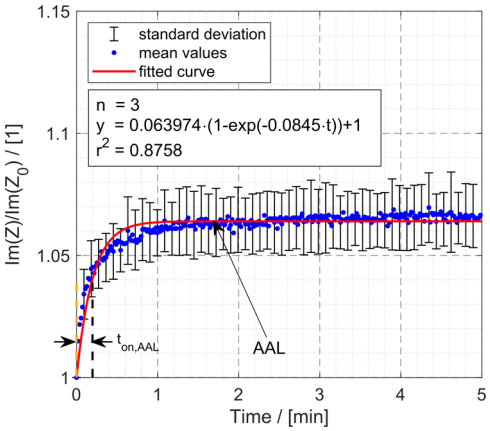

Figure 3. AAL incubation in the first 5 min. The sampling rate of the EIS measurements is increased. The imaginary part at 400 Hz is normalized to the first value obtained during the incubation step (experiment 2A). The values are averaged and the standard deviation is indicated by the error bars (n = 3). The fitted function is added (red line), and the parameters are shown in the inset including the coefficient of determination r^2. The t_{on} value is depicted in the graph.

the normalized signal obtained during the first 5 min of incubation. The additional measurement with a high time resolution was carried out three times, and the values were averaged. According to eq 2, an exponential fit function was obtained and added to the graph. A fast increase of about 6.4% in the signal is observed during the first seconds, followed by a clear saturation. This saturation is in good agreement with the "flat line" observed in Figure S6, when measurements were only taken every minute approximately (undersampling). The time constant derived according to eq 2 was determined to be $t_{on,AAL}$ = 11.8 s. In the displacement experiment (Scheme 1; 2A), a high Fuc concentration (400 mM) was applied after AAL incubation. As expected, the signal started to decrease, as depicted in Figure 4. Also, an exponential fit is added to the

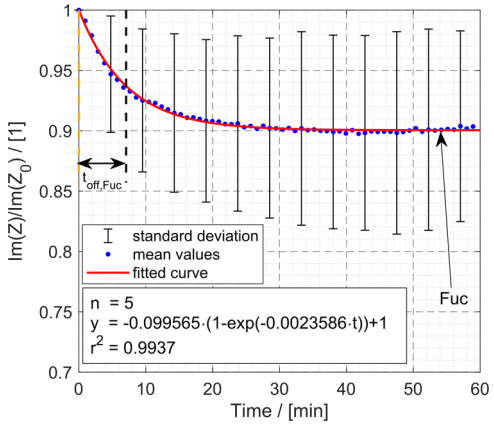

Figure 4. Relative impedance with respect to time for displacement reaction by applying Fuc after AAL incubation. The normalized imaginary part of the electrical impedance at 400 Hz during incubation of Fuc after AAL incubation (experiment 2A) exhibits a decreasing trend. The values are averaged, and the standard deviation is indicated by the error bars (n = 5). The fitted function is added (red line). The parameters are shown in the inset including the coefficient of determination r^2. The t_{off} value is depicted in the graph.

graph according to eq 1 bearing a negative A value due to the monotonically decreasing trend. k_{off} instead of k_{on} and t_{off} instead of t_{on} are the parameters describing the breaking of the complex.

It can be denoted that the signal decrease perfectly fits an exponential decay of first order and that a steady state is reached around a value of the relative impedance of 0.9. The error bars are comparatively high. The time constant $t_{off,Fuc}$ is determined to be 424 s (Table 2). In the competitive experiment (Scheme 1, 2B), 0.5 μg/mL AAL and 400 mM Fuc were simultaneously incubated in five experiments on the Le^x–NGP primed surface. Here, the binding signal only increased by less than 3.5% (Figure S9) after 60 min incubation time. The time constant is calculated to be $t_{on,AAL+Fuc}$ = 978 s and is significantly higher than $t_{on,AAL}$ (Table 2).

All obtained time constants are summarized in Table 2 for better comparison.

DISCUSSION

The development of glycan-based biosensors is an important approach for the detection of cancerogenic or pathogenic proteins. For sensitive detection, strong attractive forces between glycan and protein are crucial. Furthermore, an appropriate sensor setup and measurement technique are mandatory. To achieve a well-performing biosensor, we took advantage of a multivalent glycan presentation and the sensitivity of the EIS measurement technique. When microstructured IDEs are used, an increased signal-to-noise ratio compared with unstructured electrodes is achieved. It was recently shown by Kremers et al. that the coating of the combined CE/RE with PPy:PSS in a two-electrode arrangement reveals a significant improvement of signal stability.[24] In this work, we separated the CE and RE to a three-electrode setup and extended the idea of PPy:PSS coating to create a standalone pseudo-RE on-chip. The separation of CE and RE

https://dx.doi.org/10.1021/acssensors.0c02206
ACS Sens. 2021, 6, 1003−1011

yields additional stability because of the decoupling of the current path (CE to WE) and the voltage measurement between RE and WE. The CE and RE are both coated with PPy:PSS to obtain stable EIS measurements. The enhanced stability of the EIS signal is achieved by increasing the effective area of the CE due to the porous PPy:PSS film.[24] A volumetric capacity arises, lowering the interface impedance of the electrode in the desired frequency regime. Because of this fact, the CE can deliver enough current, which is the main requirement for this type of an electrode. In contrast to CE requirements, the RE should exhibit a constant electrode potential. Here, the PPy:PSS coating improves the stability of the open circuit potential (OCP), as investigated in a previous study in detail.[24] Because of symmetrical reasons, the two RE areas are in the arrangement and shorted off-chip. Using the entire space of the circular sensor region increases the area of the RE. The increased macroscopic area combined with the enhanced surface area due to the porous nature of the PPy:PSS coating decreases the current density at RE by orders of magnitude, causing no additional (small signal) voltage drop superposing the constant OCP.[40] Because of the electrode coating, specific binding is prohibited on these electrodes. Thus, additional stability is achieved at the CE and RE.[23] We assume that the additional use of Pluronic F-68, which is commonly used to avoid biofouling on hydrophobic surfaces, prevents unspecific binding to the polymer-based electrodes as well.[29] The final sensor design exhibits a WE made of gold where biomolecules can be immobilized easily via thiol bonds.[23]

To increase the binding efficiency of proteins and glycans, the latter were coupled to BSA as a scaffold, yielding NGPs. Twenty-five LacNAc residues were attached to the BSA and are accessible for binding of lectins and glycosyltransferases. Because lectins comprise a carbohydrate recognition domain that is repetitive, one protein can bind to several glycans at once and hence enhance the binding strength.[9] Therefore, NGPs are a promising material for glycan-based biosensors. There are different techniques to adhere NGPs to the sensor surface. In our previous paper,[23] we used a biotin−streptavidin network to functionalize the gold surface of the chip. Still, this approach constitutes problems. The application of other biotinylated proteins leads to cross-reactions between the various biotin and streptavidin layers as shown in preliminary experiments. Therefore, we decided to attach the NGP directly to the gold surface via covalent bonds. While the NGPs were functionalized via an alkyne-carrying NHS ester, the chips' gold surface was coated with an azide-PEG-thiol. The thiol binds covalently to the gold and can be easily released by the electrode cleaning procedure presented.[38] Hence, the gold chip can be used multiple times. In the next step, azide-SAM−primed gold surface and alkyne-functionalized NGPs reacted via CuAAC. The success of this reaction as well as the accessibility of the glycans for the FucT and the lectins was confirmed in preliminary tests (see Supporting Information). We concluded that an NGP glycan library can be assembled (encoded) by on-chip enzymatic glycosylation and decoded by specific lectins on a gold surface. Compared to microtiter plate-adsorbed NGPs[8] and glycan microarrays,[41−46] the gold surface offers the possibility for the detection of each modification step on the EIS biosensor.[47] Strikingly, with the EIS sensor, we were able to investigate the time-dependent protein−ligand interaction. Usually, K_d values—concentration-dependent—are the values of choice to describe the ligand binding behavior of a protein. For understanding binding processes completely, time is another crucial factor during this process.[48] k_{on} and k_{off} are the rate constants, describing the duration of the complex formation between ligand and protein and the life span of the complex, respectively. To get a better impression of these values, we took the reciprocal values of both constants that represent an actual time span (t_{on} and t_{off}). While the work of Xie et al.[13] only presents electrical characterization after each binding step by CV and EIS, our approach enables monitoring of the binding and reaction kinetics, obtaining a time−yield curve. Comparing the EIS measurements of the single incubation steps, the time constants of the NGPs binding to the gold surface and of the FucT binding to the NGPs' glycans are high, 11.9 and 18.7 min, respectively. Most importantly, our data demonstrate for the first time the kinetic monitoring of a GT reaction on a multivalent substrate. This is reflected by relatively low reaction rates with k_{cat} values describing the enzyme's turnover number, classifying Leloir-type GTs as relatively slow enzymes. *H. pylori* wildtype α3FucTs exhibit a k_{cat} of 1.1 to 7.9 s^{-1} for saturation of the active site with the substrate LacNAc.[49,50] The FucT signal directly monitors the substrate (LacNAc) conversion on a multivalent substrate to form the Le^x glycan. However, the substrate saturation is not reached. We conclude that EIS biosensors facilitate the direct kinetic deconvolution of GT reactions on immobilized NGPs. Our protocol shall be applicable to immobilize glycoproteins with trimmed glycan patterns to screen for suitable GTs for in vitro re-glycosylation of therapeutic proteins. Last but not least, the EIS biosensor setup should also be helpful for the detection of GTs in pathogenic bacteria and for the screening of bacterial toxins.[8]

For further verification of the fucosyltransfer, AAL was incubated on the Le^x-NGP primed sensors, and it exhibits a rapid binding process with only $t_{on,AAL}$ = 11.8 s. On the one hand, this shows that lectin binding is an extremely fast process. On the other hand, it verifies the activity of the applied FucT. Moreover, the 93-fold faster time constant for AAL compared to FucT offers the possibility for simultaneous incubation of FucT and AAL with the FucT reaction as the rate-limiting step. Further proof provides AAL binding to Le^x-NGP when challenged either post-binding (displacement) or during binding (competitive inhibition). The process for the displacement of AAL from the Le^x-NGP is very slow ($t_{off,Fuc}$ = 7.1 min), indicating that the monovalent Fuc can only detach AAL from the multivalent Le^x glycan ligand when applied in high excess. Furthermore, the error bars of this measurement are comparably high. Detachment of an already bound lectin is difficult to measure: The process is slower and less stable as binding processes because of the dynamic equilibrium between surface bound and detached AAL. When binding of AAL is competed in the presence of a high Fuc concentration, only a small amount of the lectin can bind because the Fuc blocks most of the binding sites of AAL. This mirrors in a t_{on} value of 16.3 min being 83-fold higher compared to the (not competed) AAL binding time constant and a significantly lower relative change of the signal. AAL comprises two identical subunits with binding pockets for five Fuc residues each.[47] This leads to a high uptake of Fuc by the lectin, leaving only a small amount of lectin binding sites for immobilized Le^x-NGPs.

In summary, layers of different biomolecules were immobilized on an IDE-based biosensor, bearing a bare gold WE, while CE and RE were coated with PPy:PSS. Thus, we

https://dx.doi.org/10.1021/acssensors.0c02206
ACS Sens. 2021, 6, 1003−1011

ensured the following aspects: (1) straight forward immobilization of biomolecules using gold-thiol bonds and (2) highly stable EIS measurements for on-line monitoring of binding kinetics. These two key features were implemented on-chip where the sensor area is only 750 μm in diameter. If necessary, the size can be further decreased for the integration in lab-on-a-chip systems. By using a broad-range toolbox of GTs and lectins, an extensive library of glycans can be established and screened with a variety of relevant carbohydrate-binding proteins in future applications. While lectin sensors already have been developed (e.g., on micro arrays), GT sensors are completely new, illustrating the action of enzymes. In further research activities, we aim for the kinetic monitoring of FucT activity by EIS embedded in a recently developed DMF system, allowing precise control of low sample volumes and rapid real-time analysis.[51] These capabilities can be utilized for instant encoding and decoding of information transmitted by the glycan code.

CONCLUSIONS

In our work, enzymatic glycosylation of NGPs on a biosensor chip was coupled for the first time with EIS measurements. The binding behavior of the different biomolecules constituting a layer-stack formation on the chips was analyzed as a first proof of concept. Further, we successfully showed discrimination between different biological recognition processes—competitive binding of lectins and their release. We expect that kinetic monitoring of on-chip NGP glycosylation via EIS can enable high-throughput screening capabilities toward diagnostic applications (cancer diagnostics, pathogen and toxin detection, and drug screening). Selectivity can be further elaborated by specific glycans addressing the substrate affinities of glycosyltransferases. Sensitivity may be enhanced by immobilization of natural multivalent glycoproteins carrying multiantennary glycans. In combination with appropriate lectins, nonspecific binding events are avoided. The improved selectivity will also enhance the sensitivity as well as the dynamic range of the sensor performance. Sensitivity can additionally be boosted by an increase of porosity (specific surface area) of the WE, decreasing the limit of detection.[16] The described additional sensor optimization will be the focus of future research.

ASSOCIATED CONTENT

Supporting Information

The Supporting Information is available free of charge at https://pubs.acs.org/doi/10.1021/acssensors.0c02206.

Compound analysis, protocol development in microtiter plates, FucT reaction scheme, verification of CuAAC in a plate, and additional EIS data (PDF)

AUTHOR INFORMATION

Corresponding Authors

Uwe Schnakenberg − *Chair of Micro- and Nanosystems and Institute of Materials in Electrical Engineering 1, RWTH Aachen University, D-52074 Aachen, Germany;* orcid.org/0000-0002-2251-0605; Phone: +49 241 80 27842; Email: schnakenberg@iwe1.rwth-aachen.de

Lothar Elling − *Laboratory for Biomaterials, Institute for Biotechnology and Helmholtz-Institute for Biomedical Engineering, RWTH Aachen University, D-52074 Aachen, Germany;* orcid.org/0000-0002-3654-0397; Phone: +49 241 80 28350; Email: l.elling@biotec.rwth-aachen.de

Authors

Viktoria Heine − *Laboratory for Biomaterials, Institute for Biotechnology and Helmholtz-Institute for Biomedical Engineering, RWTH Aachen University, D-52074 Aachen, Germany;* orcid.org/0000-0002-8667-3059

Tom Kremers − *Chair of Micro- and Nanosystems and Institute of Materials in Electrical Engineering 1, RWTH Aachen University, D-52074 Aachen, Germany;* orcid.org/0000-0003-0327-1757

Nora Menzel − *Laboratory for Biomaterials, Institute for Biotechnology and Helmholtz-Institute for Biomedical Engineering and Chair of Micro- and Nanosystems and Institute of Materials in Electrical Engineering 1, RWTH Aachen University, D-52074 Aachen, Germany*

Complete contact information is available at: https://pubs.acs.org/10.1021/acssensors.0c02206

Author Contributions

V.H. and T.K. contributed equally to the work. T.K., N.M., and V.H. performed the experiments; T.K. and V.H. wrote the manuscript; L.E. and U.S. supervised the study; all authors revised the manuscript for important intellectual content; all authors have approved to the final version of the manuscript.

Notes

The authors declare no competing financial interest.

ACKNOWLEDGMENTS

The authors express their sincere thanks to Jochen Heiß, Dorothee Breuer, and Ewa-Janina Sekula for their assistance with sensor fabrication; Lea Hansmann for valuable preliminary work during her bachelor thesis; and David Vrbata for his support with illustrations. V.H. and L.E. acknowledge support by the Collaborative Research Center (CRC) grant SFB 985 project C3 from DFG (Deutsche Forschungsgemeinschaft).

REFERENCES

(1) Christie, M. P.; Toth, I.; Simerská, P. Biophysical characterization of lectin-glycan interactions for therapeutics, vaccines and targeted drug-delivery. *Future Med. Chem.* **2014**, *6*, 2113−2129.

(2) Cui, F.; Xu, Y.; Wang, R.; Liu, H.; Chen, L.; Zhang, Q.; Mu, X. Label-free impedimetric glycan biosensor for quantitative evaluation interactions between pathogenic bacteria and mannose. *Biosens. Bioelectron.* **2018**, *103*, 94−98.

(3) Hushegyi, A.; Pihíková, D.; Bertok, T.; Adam, V.; Kizek, R.; Tkac, J. Ultrasensitive detection of influenza viruses with a glycan-based impedimetric biosensor. *Biosens. Bioelectron.* **2016**, *79*, 644−649.

(4) Hideshima, S.; Hayashi, H.; Hinou, H.; Nambuya, S.; Kuroiwa, S.; Nakanishi, T.; Momma, T.; Nishimura, S.-I.; Sakoda, Y.; Osaka, T. Glycan-immobilized dual-channel field effect transistor biosensor for the rapid identification of pandemic influenza viral particles. *Sci. Rep.* **2019**, *9*, 11616.

(5) Lazar, J.; Park, H.; Rosencrantz, R. R.; Böker, A.; Elling, L.; Schnakenberg, U. Evaluating the thickness of multivalent glycopolymer brushes for lectin binding. *Macromol. Rapid Commun.* **2015**, *36*, 1472−1478.

(6) Lazar, J.; Rosencrantz, R. R.; Elling, L.; Schnakenberg, U. Simultaneous electrochemical impedance spectroscopy and localized surface plasmon resonance in a microfluidic chip: New insights into the spatial origin of the signal. *Anal. Chem.* **2016**, *88*, 9590−9596.

(7) Rosencrantz, R. R.; Nguyen, V. H.; Park, H.; Schulte, C.; Böker, A.; Schnakenberg, U.; Elling, L. Lectin binding studies on a

glycopolymer brush flow-through biosensor by localized surface plasmon resonance. *Anal. Bioanal. Chem.* **2016**, *408*, 5633−5640.
(8) Heine, V.; Boesveld, S.; Pelantová, H.; Křen, V.; Trautwein, C.; Strnad, P.; Elling, L. Identifying EfficientClostridium difficileToxin A Binders with a Multivalent Neo-Glycoprotein Glycan Library. *Bioconjugate Chem.* **2019**, *30*, 2373−2383.
(9) Laaf, D.; Bojarová, P.; Elling, L.; Křen, V. Galectin-Carbohydrate Interactions in Biomedicine and Biotechnology. *Trends Biotechnol.* **2019**, *37*, 402−415.
(10) Josenhans, C.; Müthing, J.; Elling, L.; Bartfeld, S.; Schmidt, H. How bacterial pathogens of the gastrointestinal tract use the mucosal glyco-code to harness mucus and microbiota: New ways to study an ancient bag of tricks. *Int. J. Med. Microbiol.* **2020**, *310*, 151392.
(11) Kizuka, Y.; Taniguchi, N. Enzymes for N-glycan branching and their genetic and nongenetic regulation in cancer. *Biomolecules* **2016**, *6*, 25.
(12) Wu, Y.; Chen, X.; Wang, S.; Wang, S. Advances in the relationship between glycosyltransferases and multidrug resistance in cancer. *Clin. Chim. Acta* **2019**, *495*, 417−421.
(13) Xie, S.; Wang, F.; Wu, Z.; Joshi, L.; Liu, Y. A sensitive electrogenerated chemiluminescence biosensor for galactosyltransferase activity analysis based on a graphitic carbon nitride nanosheet interface and polystyrene microsphere-enhanced responses. *RSC Adv.* **2016**, *6*, 32804−32810.
(14) Bertok, T.; Gemeiner, P.; Mikula, M.; Gemeiner, P.; Tkac, J. Ultrasensitive impedimetric lectin based biosensor for glycoproteins containing sialic acid. *Microchim. Acta* **2013**, *180*, 151−159.
(15) Bertok, T.; Sediva, A.; Katrlik, J.; Gemeiner, P.; Mikula, M.; Nosko, M.; Tkac, J. Label-free detection of glycoproteins by the lectin biosensor down to attomolar level using gold nanoparticles. *Talanta* **2013**, *108*, 11−18.
(16) Daniels, J. S.; Pourmand, N. Label-free impedance biosensors: Opportunities and challenges. *Electroanalysis* **2007**, *19*, 1239−1257.
(17) Hu, Y.; Zuo, P.; Ye, B.-C. Label-free electrochemical impedance spectroscopy biosensor for direct detection of cancer cells based on the interaction between carbohydrate and lectin. *Biosens. Bioelectron.* **2013**, *43*, 79−83.
(18) Kluková, L.; Bertok, T.; Kasák, P.; Tkac, J. Nanoscale-controlled architecture for the development of ultrasensitive lectin biosensors applicable in glycomics. *Anal. Methods* **2014**, *6*, 4922−4931.
(19) La Belle, J. T.; Gerlach, J. Q.; Svarovsky, S.; Joshi, L. Label-Free Impedimetric Detection of Glycan−Lectin Interactions. *Anal. Chem.* **2007**, *79*, 6959−6964.
(20) Randviir, E. P.; Banks, C. E. Electrochemical impedance spectroscopy: an overview of bioanalytical applications. *Anal. Methods* **2013**, *5*, 1098−1115.
(21) Yang, L.; Li, Y. AFM and impedance spectroscopy characterization of the immobilization of antibodies on indium−tin oxide electrode through self-assembled monolayer of epoxysilane and their capture of Escherichia coli O157: H7. *Biosens. Bioelectron.* **2005**, *20*, 1407−1416.
(22) Van Gerwen, P.; Laureyn, W.; Laureys, W.; Huyberechts, G.; Op De Beeck, M.; Suls, J.; Sansen, W.; Jacobs, P.; Hermans, L.; Mertens, R. Nanoscaled interdigitated electrode arrays for biochemical sensors. *Sens. Actuators, B* **1998**, *49*, 73−80.
(23) Kremers, T.; Menzel, N.; Freitag, F.; Laaf, D.; Heine, V.; Elling, L.; Schnakenberg, U. Electrochemical Impedance Spectroscopy Using Interdigitated Gold-Polypyrrole Electrode Combination. *Phys. Status Solidi* **2020**, *217*, 1900827.
(24) Kremers, T.; Tintelott, M.; Pachauri, V.; Vu, X. T.; Ingebrandt, S.; Schnakenberg, U. Microelectrode Combinations of Gold and Polypyrrole Enable Highly Stable Two-electrode Electrochemical Impedance Spectroscopy Measurements under Turbulent Flow Conditions. *Electroanalysis* **2020**, *33*, 197.
(25) Sauerzapfe, B.; Namdjou, D.-J.; Schumacher, T.; Linden, N.; Křenek, K.; Křen, V.; Elling, L. Characterization of recombinant fusion constructs of human β1,4-galactosyltransferase 1 and the lipase pre-propeptide from Staphylococcus hyicus. *Staphylococcus hyicus. J. Mol. Catal. B: Enzym.* **2008**, *50*, 128−140.
(26) Choi, Y. H.; Kim, J. H.; Park, B. S.; Kim, B.-G. Solubilization and Iterative Saturation Mutagenesis of α1, 3-fucosyltransferase from Helicobacter pylori to enhance its catalytic efficiency. *Biotechnol. Bioeng.* **2016**, *113*, 1666−1675.
(27) Sauerzapfe, B.; Křenek, K.; Schmiedel, J.; Wakarchuk, W. W.; Pelantová, H.; Křen, V.; Elling, L. Chemo-enzymatic synthesis of poly-N-acetyllactosamine (poly-LacNAc) structures and their characterization for CGL2-galectin-mediated binding of ECM glycoproteins to biomaterial surfaces. *Glycoconjugate J.* **2009**, *26*, 141−159.
(28) Laaf, D.; Bojarová, P.; Pelantová, H.; Křen, V.; Elling, L. Tailored multivalent neo-glycoproteins: Synthesis, evaluation, and application of a library of galectin-3-binding glycan ligands. *Bioconjugate Chem.* **2017**, *28*, 2832−2840.
(29) Au, S. H.; Kumar, P.; Wheeler, A. R. A new angle on pluronic additives: advancing droplets and understanding in digital microfluidics. *Langmuir* **2011**, *27*, 8586−8594.
(30) Hoffmann, M.; Hayes, M. R.; Pietruszka, J.; Elling, L. Synthesis of the Thomsen-Friedenreich-antigen (TF-antigen) and binding of Galectin-3 to TF-antigen presenting neo-glycoproteins. *Glycoconjugate J.* **2020**, *37*, 457.
(31) Hong, V.; Presolski, S. I.; Ma, C.; Finn, M. G. Analysis and Optimization of Copper-Catalyzed Azide-Alkyne Cycloaddition for Bioconjugation. *Angew. Chem.* **2009**, *121*, 10063−10067.
(32) El Hasni, A.; Schmitz, C.; Bui-Göbbels, K.; Bräunig, P.; Jahnen-Dechent, W.; Schnakenberg, U. Electrical impedance spectroscopy of single cells in hydrodynamic traps. *Sens. Actuators, B* **2017**, *248*, 419−429.
(33) Li, C. M.; Sun, C. Q.; Chen, W.; Pan, L. Electrochemical thin film deposition of polypyrrole on different substrates. *Surf. Coat. Technol.* **2005**, *198*, 474−477.
(34) Brandl, V.; Holze, R. Influence of the preparation conditions on the properties of electropolymerised polypyrrole. *Ber. Bunsenges. Phys. Chem.* **1998**, *102*, 1032−1038.
(35) Cui, X.; Hetke, J. F.; Wiler, J. A.; Anderson, D. J.; Martin, D. C. Electrochemical deposition and characterization of conducting polymer polypyrrole/PSS on multichannel neural probes. *Sens. Actuators, A* **2001**, *93*, 8−18.
(36) Dorledo de Faria, R. A.; Dias Heneine, L. G.; Matencio, T.; Messaddeq, Y. Faradaic and non-faradaic electrochemical impedance spectroscopy as transduction techniques for sensing applications. *Int. J. Biosens. Bioelectron.* **2019**, *5*, 29−31.
(37) Lazar, J.; Schnelting, C.; Slavcheva, E.; Schnakenberg, U. Hampering of the stability of gold electrodes by ferri-/ferrocyanide redox couple electrolytes during electrochemical impedance spectroscopy. *Anal. Chem.* **2015**, *88*, 682−687.
(38) Kim, D. J.; Pitchimani, R.; Snow, D. E.; Hope-Weeks, L. J. A simple method for the removal of thiols on gold surfaces using an NH4OH−H2O2−H2O solution. *Scanning* **2008**, *30*, 118−122.
(39) Tanak, A. S.; Jagannath, B.; Tamrakar, Y.; Muthukumar, S.; Prasad, S. Non-Faradaic electrochemical impedimetric profiling of procalcitonin and C-Reactive protein as a dual marker biosensor for early sepsis detection. *Anal. Chim. Acta: X* **2019**, *3*, 100029.
(40) Lvovich, V. F. *Impedance Spectroscopy: Applications to Electrochemical and Dielectric Phenomena*; John Wiley & Sons, 2012.
(41) Gray, C. J.; Sánchez-Ruíz, A.; Šardzíková, I.; Ahmed, Y. A.; Miller, R. L.; Reyes Martinez, J. E.; Pallister, E.; Huang, K.; Both, P.; Hartmann, M.; Roberts, H. N.; Šardzík, R.; Mandal, S.; Turnbull, J. E.; Eyers, C. E.; Flitsch, S. L. Label-free discovery array platform for the characterization of glycan binding proteins and glycoproteins. *Anal. Chem.* **2017**, *89*, 4444−4451.
(42) Gray, C. J.; Weissenborn, M. J.; Eyers, C. E.; Flitsch, S. L. Enzymatic reactions on immobilised substrates. *Chem. Soc. Rev.* **2013**, *42*, 6378−6405.
(43) Peng, W.; Nycholat, C. M.; Razi, N.., Glycan microarray screening assay for glycosyltransferase specificities. *Glycosyltransferases*; Springer, 2013; pp 1−14.

(44) Prudden, A. R.; Liu, L.; Capicciotti, C. J.; Wolfert, M. A.; Wang, S.; Gao, Z.; Meng, L.; Moremen, K. W.; Boons, G.-J. Synthesis of asymmetrical multiantennary human milk oligosaccharides. *Proc. Natl. Acad. Sci. U.S.A.* **2017**, *114*, 6954−6959.
(45) Serna, S.; Etxebarria, J.; Ruiz, N.; Martin-Lomas, M.; Reichardt, N.-C. Construction of N-Glycan Microarrays by Using Modular Synthesis and On-Chip Nanoscale Enzymatic Glycosylation. *Chem.—Eur. J.* **2010**, *16*, 13163−13175.
(46) Serna, S.; Hokke, C. H.; Weissenborn, M.; Flitsch, S.; Martin-Lomas, M.; Reichardt, N.-C. Profiling glycosyltransferase activities by tritium imaging of glycan microarrays. *ChemBioChem* **2013**, *14*, 862−869.
(47) Wimmerova, M.; Mitchell, E.; Sanchez, J.-F.; Gautier, C.; Imberty, A. Crystal Structure of Fungal Lectin Six-Bladed β-Propeller Fold and Novel Fucose Recognition Mode for Aleuria Aurantia Lectin. *J. Biol. Chem.* **2003**, *278*, 27059−27067.
(48) Corzo, J. Time, the forgotten dimension of ligand binding teaching. *Biochem. Mol. Biol. Educ.* **2006**, *34*, 413−416.
(49) Ma, B.; Audette, G. F.; Lin, S.; Palcic, M. M.; Hazes, B.; Taylor, D. E. Purification, kinetic characterization, and mapping of the minimal catalytic domain and the key polar groups of Helicobacter pylori α-(1, 3/1, 4)-fucosyltransferases. *J. Biol. Chem.* **2006**, *281*, 6385−6394.
(50) Tan, Y.; Zhang, Y.; Han, Y.; Liu, H.; Chen, H.; Ma, F.; Withers, S. G.; Feng, Y.; Yang, G. Directed evolution of an α1, 3-fucosyltransferase using a single-cell ultrahigh-throughput screening method. *Sci. Adv.* **2019**, *5*, No. eaaw8451.
(51) Kremers, T.; Thelen, S.; Bosbach, N.; Schnakenberg, U. PortaDrop: A portable digital microfluidic platform providing versatile opportunities for Lab-On-A-Chip applications. *PLoS One* **2020**, *15*, No. e0238581.

https://dx.doi.org/10.1021/acssensors.0c02206
ACS Sens. 2021, 6, 1003−1011